View metadata, citation and similar papers at core.ac.uk
brought to you by CORE
provided by Ghent University Academic Bibliography

LOCAL DAMAGE IN A 5 – HARNESS SATIN WEAVE COMPOSITE UNDER STATIC TENSION: PART II - MESO – FE MODELLING

S. Daggumati [a], W. Van Paepegem[a], J. Degrieck[a], J. Xu[b], S.V. Lomov[b], I. Verpoest[b]*

[a]Ghent University, Dept. of Materials Science and Engineering, Sint-Pietersnieuwstraat 41, 9000 Gent, Belgium

[b]Katholieke Universiteit Leuven, Department of Metallurgy and Materials Engineering, Kasteelpark Arenberg 44, B-3001 Leuven, Belgium

ABSTRACT

This study forms the second part of a paper on the local damage analysis in a thermo-plastic 5-harness satin weave composite under uni-axial static tensile load. The experimental observations of Part I are confronted with the meso-FE simulations. Part II describes the following steps regarding the unit cell meso-FE modeling starting from: 1) Construction of the unit cell geometrical model; 2) Estimation of the homogenized elastic constants of the unit cell using different boundary conditions; 3) Evaluation of the local stress and damage behavior of the unit cell using meso-FE simulations. The aim of the numerical analysis is to investigate the dependency of local ply stress and damage profiles on the adjacent layers of the laminate.

---

*Corresponding author. Tel.: +32 92 64 33 17; fax: +32 92 64 35 87.

E-mail address: Subbareddy.Daggumati@ugent.be

In order to reflect the constraints posed by the surrounding plies, depending on the ply placement in the laminate (inside / surface), different unit cell geometrical models with suitable boundary conditions were used for the FE analysis. From the numerical simulations it is observed that: a) the homogenized elastic constants of the unit cell vary considerably depending on the boundary conditions used for the unit cell FE analysis; b) intra-yarn stress and damage profiles are sensitive to the unit cell model as well as the boundary conditions used for the FE analysis.

Keywords: Textile composites, Finite element analysis (FEA), Damage mechanics, Weft yarn damage, Multiscale modeling.

1. Introduction

In order to estimate the homogenized elastic constants of textile composites using unit cell meso-FE simulations, a numerical procedure is firmly established [1, 2]. However, the meso-FE procedure still needs to be improved for analysis of the local stress and damage behavior of the composite using the unit cell FE simulations [3, 4]. The majority of the published numerical work regarding the analysis of local structural behavior in the textile composite is based on the single unit cell FE simulation with 3D PBCs (Periodic Boundary Conditions). The underlying principle in the application of 3D PBCs is that the unit cell is chosen from the middle of the laminate [5-8], which represents the entire stress/strain fields in the composite.

However, recent publications [9-11] on the meso-FE analysis of the unit cell have emphasized the effect of free surface and free edges on local stress behavior. Moreover, the influence of internal yarn shifting on the local stress behavior of the unit cell has been highlighted. In order to investigate the effect of local fabric geometries on the damage behaviour, Le Page et al.[12] developed two dimensional plane strain FE models of woven composite with in-phase, out-of-phase and staggered nested unit cell models. The above mentioned work concluded that the strain energy release rate associated with the crack formation is influenced significantly by the crack location. In addition, the formation of a crack is associated with the local bending deformation, and the energy release rate increases with the degree of bending. According to Adams et al.[13], the modelling approaches assume idealized textile architecture and generally consider a single unit cell. Due to the randomness of textile architecture produced using conventional processing techniques, the experimental data obtained has shown limited use for verifying the accuracy of these numerical models.

In the above context, Part I of this paper described the experimental observations of the sequence of damage events in different layers of the 5-harness satin weave carbon-PPS laminate, which are influenced by the local fabric geometries. Weft yarn transverse damage is initiated in the inner layers of the laminate, followed by damage on the surface layers. The sequence of damage events in different layers implies that the damage initiation may have been influenced by the local constraints imposed by the surrounding plies. In Part II of this paper, the above experimental observation is verified using the unit

cell as well as laminate level 3D meso-FE simulations. The work presented here is conducted in the view of obtaining extensive knowledge on the mechanics of the local structural behaviour of a satin weave composite.

2. Estimation of the homogenized elastic constants

2.1. Construction of the unit cell FE model

In order to begin with the homogenization of elastic constants and the simulation of the local structural behavior on the meso scale, the textile reinforcement under consideration should be accurately constructed and translated to the FE software. The micro-CT technique is employed to investigate the variability of the internal yarn dimensions in a processed composite. To quantify the variation of the internal yarn dimensions in multiple composite samples at the same time, three laminates were taped together each with the dimensions of $10.4 \times 10.4 \times 2.5$ mm and this stack was used for the micro-CT analysis. The size of the composite samples used for the micro-CT is determined according to the optimum dimensions of the unit cell. The output micro-CT images were reconstructed and used for the measurement of the textile parameters.

The textile information required for the construction of unit cell geometry such as the spacing, width and thickness of the yarns are measured at 20 different locations in both the warp and weft directions of the micro-CT images. The averaged values are shown in Table 1. Using the data from Table 1, the unit cell geometric model of the 5 - harness

satin weave reinforcement is generated using the ‘WiseTex’ software [14, 15]. Later, the ‘WiseTex’ generated textile reinforcement is transferred into FE mesh and filled with the matrix using the ‘MeshTex’ software [5]. Finally, the ‘MeshTex’ output in the form of nodal and elemental information is transferred to the ABAQUS software.

2.2. Homogenization of the elastic constants

In order to start the unit cell FE analysis, the micro-mechanical (UD) material properties of the carbon-PPS representing the homogenized material properties of the impregnated yarn are derived from the individual elastic properties of the carbon fibre and PPS matrix (Table 2) using the analytical Chamis [16] homogenization formulas. The intra-yarn volume fraction (ϕ_f) used for the calculation of the homogenized material properties (Table 3) is 70% (constant through out the yarn sections), which is obtained from the ‘WiseTex’ software. The analytical homogenized elastic constants of the impregnated yarn are compared with the CCA [17] and show good correlation. The calculated homogenized micro-mechanical material properties are assigned to the yarn cross sections in their local co-ordinate system to account for the yarn crimp in the FE model. Moreover, perfect bonding is assumed at the interface between the yarns and matrix of the unit cell: i.e. the yarn and the matrix share common node at the interface, which has been justified by Gerlach et al. [18].

The effective elastic constants of the textile composite on the scale of a single unit cell are calculated using the numerical meso-mechanical homogenization procedure. Initially, the elastic constants of the composite on the meso scale are estimated by applying the

Dirichlet boundary conditions to the unit cell. The procedure involved in the estimation of elastic constants using the Dirichlet boundary conditions is explained in [19, 20]. In order to calculate the homogenized elastic constants of the unit cell, FE analysis is started by solving 6 independent unit load cases (3 normal $\varepsilon_x, \varepsilon_y, \varepsilon_z$ and 3 shear $\gamma_{xy}, \gamma_{xz}, \gamma_{yz}$ strains), thereby calculating the $[AD]$ parts of the $[ABD]$ stiffness matrix. By inverting the $[AD]$ stiffness matrix, the compliance components of the unit cell were obtained. From this, nine homogenized elastic constants of the unit cell are computed (Table 4).

The other procedure used for the evaluation of the homogenized elastic constants of the unit cell is periodic boundary conditions (PBCs) [5, 21-23] along with the volume averaging technique. By applying the 3D PBC, the above mentioned six independent unit load cases are solved. Later, by the application of the volume averaging technique [1, 5, 24], the homogenized elastic constants of the unit cell are estimated (Table 4). Finally, the elastic constants computed using different boundary conditions are compared to the analytical (method of inclusions [25]) and with the experimental elastic constants (Table 4).

The difference in the estimated values of the homogenized elastic constants between the periodic and Dirichlet boundary conditions has been explained by Terada et al. [2]. In correlation with the observations of the current work, the homogenized elastic properties estimated using Dirichlet boundary conditions have higher predicted values than those of the periodic boundary conditions. From the elastic constants computed with different

procedures, it is evident that the periodic boundary conditions along with the volume averaging technique predict better results compared to the experimental results.

3. Unit cell FE analysis

To start with the meso-FE damage analysis, along with the micro-mechanical elastic properties, the strength properties of the carbon-PPS UD (Table 5) are derived from the individual strength properties of the carbon fibre and PPS matrix (Table 2) using the Chamis analytical strength homogenization formulas [16]. Once the transverse isotropic strength properties to the yarns and the isotropic material properties of the matrix are assigned, for the damage analysis of the unit cell the following approach is employed.

Initially, the occurrence of damage in the unit cell element is detected using the Hoffmann failure criteria [26]. However, this criterion cannot indicate the type of damage mode in the yarns, where the architecture of the fibre arrangement plays an important role. The modes of the damage are classified into four different types (Table 6) [27]. The mode L represents the fibre breaking, T and Z modes represent the transverse and shear cracking. As shown in Table 6, by calculating the corresponding stress-to-strength ratios for the different modes, we consider that the damage mode that is taking place is the one whose stress-to-strength ratio has the maximum value. The above mentioned failure criteria and the damage model is implemented into the commercial FE software ABAQUS using UMAT Fortran routines, which enable us to simulate the damage in the unit cell.

The results obtained from the FE modeling are compared with the experimental observations as follows:

1. Validation of the FE damage initiation strain with the damage initiation strain obtained from the experimental acoustic emission technique (Part I).
2. Finding the FE damage initiation location in the unit cell, which could be verified with the microscopically observed damage initiation location on the quasi-static tensile tested composite specimen (Part I).

Finally, the local stress profiles are plotted for various unit cell models to analyze the effect of unit cell stacking and the applied boundary conditions.

CASE I: (FE simulation of the damage in the laminate inner layers)

In order to simulate the stress and damage behavior inside the laminate, FE analysis is started with a single unit cell by applying 3D PBCs [5, 22], which corresponds to the unit cell located in the middle of the laminate. During the loading process, at <0.2%> of the applied average tensile strain in the warp direction (Fig. 1 X-direction), the damage initiation is detected at the edges of the weft yarn at the yarn crimp location by Hoffmann criteria (Figure 1c). Once the Hoffmann criteria detect the damage initiation in the element, for the direction of the damage, individual stress to strength ratios are calculated using the formulas shown in the Table 6. And the values are listed below for the damaged elements.

Mode L ($\frac{\sigma_l^2}{F_L^t F_L^c}$) = Negligible Mode T ($\frac{\sigma_t^2}{F_T^t F_T^c}$) = 0.23

Mode Z ($\frac{\sigma_Z^2}{F_Z^t F_Z^c}$) = 0.08 Mode TZ $(\frac{\tau_{TZ}}{S})^2$ = 0.16
F_{TZ}

Based on the individual stress to strength ratios shown above, the local transverse damage (meso level) in a satin weave weft yarn is a combination of the micro level transverse damage mode in combination with the out-of-plane shear damage mode. The predicted FE micro level damage modes are in correlation with the theory of Cox [28] on the satin weave composite architecture. Cox reported that the asymmetric satin weave fabric causes the coupling of bending and stretching, and there is also coupling between stretching and in-plane shear under the pure tensile load. In the present case, it is observed that the load coupling between stretching and in-plane shear is negligible compared to the load coupling between bending and stretching.

From the transverse stress contours (Figure 1a), the maximum stress of 49 MPa is observed at the damaged elements of the weft yarn. Moreover, the transverse stress profile (Figure 1b) is plotted on the surface elements of the weft and warp yarns between the yarn crimp locations as marked in Figure 1a. From the Figure 1b, the variation in local transverse stress is divided into three major parts as explained below:

- Starting from the centre of the weft yarn at the yarn crimp location, the transverse stress value increases from 30 MPa to the maximum value of 49 MPa at the edge of the weft yarn.
- The second phase of the stress profile starts at the edge of the weft yarn, and decreases to the minimum value (12 MPa) in the geometrical transition location between the crimp region to the flat position of the load carrying warp yarn.
- The third phase in the stress profile is related to the constant transverse stress of 10 MPa at the flat position of the load carrying warp yarn. In addition, the stress profile varies periodically along the unit cell geometry.

CASE II: (FE simulation of the damage on the laminate surface layer)

The current section deals with the numerical simulation of the local stress and damage behavior of the unit cell on the traction free surface. In order to understand the variation in local damage behavior in the finite surface laminate compared to the infinite laminate, the single unit cell FE analysis with 3D PBCs is changed as explained below.

Initially, the surface stress analysis is performed using the single unit cell with in-plane PBCs. The top and bottom surfaces of the unit cell (Figure 2a) are free to deform in the out-of-plane direction. Under the above specified constraints, at <0.25%> of the applied average strain in the warp yarn direction, weft yarn damage is detected at the yarn crimp location (Figure 2b). From the local stress analysis, it is observed that the maximum tensile stress (80 MPa) occurs at the centre of the weft yarn (Figure 2a). Due to the absence of textile reinforcement or supporting boundary conditions in the out-of-plane

direction, the flat part of the warp yarn adjacent to the yarn crimp location is slightly compressed in the transverse direction (Figure 2c).

Comparison of the experimental (<0.6%>) and numerical (<0.25%>) surface damage initiation strains underline the necessity for improvement in the unit cell model used for the surface stress analysis. To capture the effect of underlying layers on the surface stress profile, it is necessary to create a unit cell stack for the FE analysis. However, producing the unit cell stack with the same mesh size as single unit cell is computationally expensive. In this regard, comparison of the numerical local strain profiles with different mesh densities to the experimentally measured strains by Lomov et al. [29] lead to the conclusion that, the effect of mesh size is minimal on the local strain variation. In the current work, to study the effect of mesh size on the local stress behavior, Figure 2c compares the local transverse stress profiles on the traction free surface with different unit cell mesh densities. The unit cell model with a coarse mesh has 8400 elements, and the fine mesh has 53200 elements. From the local stress curves (Figure 2c), it is evident that the maximum and minimum stress locations are the same. Further, there is a difference of approximately 10MPa stress between the fine and coarse mesh at the yarn crimp location.

In the process of improving the unit cell FE analysis, eight unit cells are stacked such that all the yarn crimp locations are in the same phase (Figure 3a). In-plane PBCs are applied to the edges of the unit cell, while the top and bottom surfaces are free to deform. With the aforementioned loading conditions, at <0.44%> of the global tensile strain in the warp

yarn direction, transverse damage is detected at the weft yarn centre in the surface layer of the unit cell (Figure 3b). In addition, the transverse stress of 75 MPa is observed in the damaged elements (Figure 3a).

3. Results and discussion

In this section, comparison between the experimental (Part I) and numerical damage analysis is presented. This section is later extended to the analysis of unit cell local stress behavior at different locations of the laminate. The experimental AE (Acoustic Emission) technique predicts the weft yarn damage in the laminate inner layers around <0.1-0.2%> of the global tensile strain in the warp yarn direction. Simulation of the single unit cell with 3D PBCs predicts the weft yarn damage around <0.2%> of the global tensile strain, which proves to be a good correlation with the experimental results considering the fact that the computational model did not consider the thermal stress in the composite. In a sense, the damage initiation strain obtained from the FE simulations is a deterministic maximum value, which is within the limits of the experimental prediction. Moreover, the damage initiation location obtained from the FE simulation at the edge of the weft yarn (Case-I) shows a good correlation with the observed microscopic damage locations.

On the traction free surface, the single unit cell with in-plane PBCs and the 8 unit cell in-phase stack predict the weft yarn damage at around <0.25%> and <0.44%> of the global tensile strain respectively. Comparison of the numerical damage initiation strain with the microscopically observed damage initiation strain on the surface (around <0.6%>) proves

that the FE simulations predict the early damage initiation strain. In correlation with the experimental damage location, the numerical simulations predict the damage at the centre of the weft yarn. Based on the comparison of the experimental and numerical results, it is evident that without the presence of internal yarn shifting (nesting), by in-phase stacking of the yarn crimp locations, the maximum out-of-plane deformation in the surface layers is reached earlier than in the experimental counterpart (with the internal yarn nesting) and hence causes the early damage initiation [4, 30].

In addition to the local damage analysis, the unit cell local stress analysis provides insight into the active stress components and their variations depending on the lamina position in the laminate. The major local stress components observed in the weft yarn at the yarn crimp location are the in-plane transverse stress (σ_{22}), the out-of-plane normal stress (σ_{33}) and the out-of-plane shear stress (σ_{23}) components for the applied global tensile strain in the warp yarn direction. The local weft yarn stress values at the yarn crimp location for the single unit cell as well as the laminate are listed in Table 7. Comparison of the stress components inside the laminate (Case I) with the surface weft yarn stresses (CASE II) shows that the restriction of the yarn crimp inside the laminate causes a higher out-of-plane shear (σ_{23}) as well as out-of-plane normal stress (σ_{33}) compared to the surface layers. The stress pattern observed above is in correlation with the research output of Lee et al.[31] on the local strain behavior of a plain weave composite. The authors reported that the tension/in-plane shear and tension/bending coupling effects at the yarn crimp inside the laminate are restricted by the surrounding plies. In contrast, the

unrestricted yarn crimp on the surface layers of the laminate caused weft yarn damage due to the maximum transverse and shear stress.

Apart from the local stress and damage analysis, studying the deformation behavior of the unit cell under the external load provides knowledge on the effect of stacking and the applied boundary conditions for the unit cell FE analysis. The literature [27, 32, 33] has shown that the tensile load applied to the unit cell causes the straightening of the yarn in the loading direction (warp). This straightening effect imposes the out-of-plane deformation on the perpendicular weft yarn. When the weft yarn deformation reaches its maximum value, damage will occur on the surface of the weft yarn. Based on the above statement, the out-of-plane deformation is plotted on the surface of the unit cell in the positive z-direction between two yarn crimp locations (dotted line in Figure 1a) at the moment of damage initiation. Considering the absolute difference from maximum to minimum deformation, as expected, the out-of-plane deformation is restricted with 3D PBCs (Figure 4a) causing an almost flat deformation starting from one yarn crimp to the other (peak points in the curves represent the yarn crossover position). In contrast, the single unit cell with in-plane PBC predicts a large difference in the out-of-plane deformation (Figure 4b) between the yarn crimp and the flat yarn position. Moreover, the absolute difference in the out-of-plane deformation value for the 8 unit cell stack (Figure 4c) at <0.44%> of the global strain is approximately twice the value of the infinite laminate at <0.2%>. The aforementioned statement shows that, by increasing the number of unit cells in the stack, the out-of-plane deformation at the yarn crimp of the finite surface unit cell stack approaches the infinite laminate deformation [9].

4. Conclusions

Part I of this paper introduced an experimental procedure for analyzing the damage initiation and the history of the damage in a 5-harness satin weave composite. The experimental procedure provided the qualitative as well as quantitative knowledge about the damage. In order to understand the stress behavior and the mechanics of damage, the current paper deals with the satin weave unit cell computational model. Numerical simulations provided insight into the mesoscopic damage locations and the stress behavior. Comparison of the experimental and simulation results lead to the following conclusions:

- The predicted FE damage initiation strain and location for the inner layers of the laminate are within the limits of the experimental observation. On the other hand, the single unit cell with 2D PBC and in-phase stacking of an 8 unit cell laminate predict the early damage initiation strain of <0.25%> and <0.44%> on the surface layers, compared to the experimental damage initiation of <0.6%>. This early damage initiation strain in the FE simulation can be attributed to the absence of internal yarn shifting in the computational model.

- The local damage initiation trend obtained from the numerical simulations demonstrates that the infinite laminate predicts early

damage initiation at the edges of the weft yarn. In contrast, the free surface unit cells predict damage in the later stage.

- In correlation with the experimental observations, the different weft yarn damage initiation strains at different locations of the laminate suggest that the transverse weft yarn damage in a textile composite is a sequential process.

- In conclusion, the effect of internal yarn shifting (nesting) on the local structural response cannot be neglected and can not be captured by the infinite laminate FE analysis.

The essence of the two parts of the current local damage analysis is summarized as follows. By observing the experimental microscopic damage phenomena on the scale of the laminate at the end of the loading process, formation of cracks in the weft yarn at different locations appear to be completely stochastic in nature. However, by segregating the entire damage mechanism at different length scales, analyzing the factors contributing to the damage on the relevant scale, following the history of the damage and using the numerical simulations, the failure mechanism in textile composites can be understood in a certain deterministic way.

ACKNOWLEDGEMENTS

The authors would like to acknowledge the FWO - Vlaanderen for the financial support provided through the project G.0233.06H. The authors also express their gratitude to ‘Ten Cate’ for supplying the composite plates.

REFERENCES

[1]. Carvelli, V. and C. Poggi, *A homogenization procedure for the numerical analysis of woven fabric composites.* Composites Part A: Applied Science and Manufacturing, 2001. **32**(10): p. 1425-1432.

[2]. Terada, K., et al., *Simulation of the multi-scale convergence in computational homogenization approaches.* International Journal of Solids and Structures, 2000. **37**(16): p. 2285-2311.

[3]. Ivanov, d.S., *Damage analysis in textile composites.* PhD Thesis; KU Leuven - Faculty of Engineering, May 2009.

[4]. Carvalho, N.V., S.T. Pinho, and P.Robinson, *Compressive failure of 2D woven composites.* ICCM-17 Conference proceedings, 2009.

[5]. Lomov, S.V., et al., *Meso-FE modelling of textile composites: Road map, data flow and algorithms.* Composites Science and Technology, 2007. **67**(9): p. 1870-1891.

[6]. Whitcomb, J.D., *Three-Dimensional Stress Analysis of Plain Weave Composites.* NASA Contractor Report 101672, 1989.

[7]. whitcomb, *Analysis of New Composite Architectures.* NASA Contractor Report 198506, 1996.

[8]. Bogdanovich, A.E., *Multi-scale modeling, stress and failure analyses of 3-D woven composites.* Journal of Materials Science, 2006.

[9]. Ivanov, D.S., et al., *Stress distribution in outer and inner plies of textile laminates and novel boundary conditions for unit cell analysis.* Composites Part A: Applied Science and Manufacturing. **In Press, Accepted Manuscript**.

[10]. Owens, B.C., J.D. Whitcomb, and J. Varghese, *Effect of Finite Thickness and Free Edges on Stresses in Plain Weave Composites*. 2009. p. 0021998309347571.

[11]. Lomov, S.V., et al., *Nesting in textile laminates: geometrical modelling of the laminate.* Composites Science and Technology, 2003. **63**(7): p. 993-1007.

[12]. Le Page, B.H., et al., *Finite element simulation of woven fabric composites.* Composites Part A: Applied Science and Manufacturing, 2004. **35**(7-8): p. 861-872.

[13]. Adams, D.O., *Idealized textile composites for experimental/analytical correlation.* NASA Technical Memorandum 19950016857 1994.

[14]. Lomov, S.V., et al., *Textile composites: modelling strategies.* Composites Part A: Applied Science and Manufacturing, 2001. **32**(10): p. 1379-1394.

[15]. Verpoest, I. and S.V. Lomov, *Virtual textile composites software WiseTex: Integration with micro-mechanical, permeability and structural analysis.* Composites Science and Technology, 2005. **65**(15-16): p. 2563-2574.

[16]. Chamis, C.C., *Mechanics of Composite Materials Past, Present, and Future.* NASA Technical Memorandum 100793, 1984.

[17]. Hofstee, J. and F. van Keulen, *Elastic stiffness analysis of a thermo-formed plain-weave fabric composite Part II: analytical models.* Composites Science and Technology, 2000. **60**(8): p. 1249-1261.

[18]. Gerlach, R., et al., *The interface between matrix pockets and fibre bundles under impact loading.* Composites Science and Technology, 2009. **69**(11-12): p. 2024-2026.

[19]. He, H., Y.C. Roth, and N. Himmel, *Elastic constants estimation of stitched NCF CFRP laminates based on a finite element unit-cell model.* Composites Science and Technology, 2007. **67**(6): p. 1081-1095.
[20]. Sun, C.T. and R.S. Vaidya, *Prediction of composite properties from a representative volume element.* Composites Science and Technology, 1996. **56**(2): p. 171-179.
[21]. C. Pellegrino, U.G.B.A.S., *Numerical homogenization of periodic composite materials with non-linear material components*. 1999. p. 1609-1637.
[22]. Chapman, C.D., *Effect of assumed Tow architecture on the predicted moduli and stress in woven composites* NASA Contractor Report 195310, 1994.
[23]. Wang, X.F., et al., *Multi-scale Analyses of 3D Woven Composite Based On Periodicity Boundary Conditions.* Journal of Composite Materials, 2006.
[24]. Carvelli, V. and A. Taliercio, *A micromechanical model for the analysis of unidirectional elastoplastic composites subjected to 3d stresses.* Mechanics Research Communications, 1999. **26**(5): p. 547-553.
[25]. Lomov, S. and I. Verpoest, *Homogenisation of a sheared unit cell of textile composite FEA and approximate inclusion model.* Department of MTM, Katholieke Universiteit Leuven, 2004.
[26]. Tolson, S. and N. Zabra, *Finite element analysis of progressive failure in laminated composite plates.* Compurers & Structures Vol. 38, No. 3, pp. 361-376, 1991, 1990.
[27]. Zako, M. and Y. Uetsuji, *On the damage behavior of fiber reinforced composite materials.* International Journal of damage mechanics, 2002.
[28]. Cox, B.N. and G. Flanagan, *Handbook of Analytical Methods for textile composite.* NASA Contractor Report 4750, 1997.
[29]. Lomov, S.V., et al., *Full-field strain measurements for validation of meso-FE analysis of textile composites.* Composites Part A: Applied Science and Manufacturing, 2008. **39**(8): p. 1218-1231.
[30]. Ivanov, D., et al., *Strain mapping analysis of textile composites.* Optics and Lasers in Engineering. **In Press, Corrected Proof**.
[31]. Lee, J.-R., et al., *Digital phase-shifting grating shearography for experimental analysis of fabric composites under tension.* Composites Part A: Applied Science and Manufacturing, 2004. **35**(7-8): p. 849-859.
[32]. Summerscales, J. and P.M. Russel, *Observations on the fibre distribution and fibre strain in a woven fabric reinforcement.* Advanced composite letters 2004. **23 No.3, 2004**.
[33]. John, S., I. Herszberg, and F. Coman, *Longitudinal and transverse damage taxonomy in woven composite components.* Composites Part B: Engineering, 2001. **32**(8): p. 659-668.
[34]. Wijskamp, S., *Shape distortion in composite forming.* PhD Thesis, University of Twente, Enschede, The Netherlands, May 2005.
[35]. De Baere, I., *Experimental and Numerical Study of Different Setups for Conducting and Monitoring Fatigue Experiments of Fibre-Reinforced Thermoplastics.* PhD Thesis, Gent university, 2008.

Table 1. Textile parameters obtained from the micro-CT measurements.

WiseTex input data at fabric level		
Property	*5 harness satin weave warp*	*5 harness satin weave weft*
Yarn	*198 tex*	
Number of measurements	*20*	*20*
Yarn width (mm)	1.31 ± 0.01	1.32 ± 0.08
Yarn thickness (mm)	0.162 ± 0.01	0.161 ± 0.06
Yarn spacing (mm)	1.50 ± 0.04	1.49 ± 0.07
WiseTex input data at fibre level		
TEX (g/km)	*198*	
Yarn filament count	*3000*	
Filament diameter (mm)	*0.007*	
Carbon fibre density (g/cm^3)	*1.75*	

Table 2. T300 JB carbon fibre, PPS elastic and strength properties.

T300 JB carbon fibre		*PPS (PolyPhenelyene Sulphide)*	
Elastic properties [5, 34]			
Longitudinal modulus E_{11}, GPa	*231*	*Modulus of elasticity E, GPa*	*3.8*
Transverse modulus E_{22}, GPa	*28*	*Shear modulus G, GPa*	*1.38*
In-plane shear modulus G_{12}, GPa	*24*	*Poisson's ratio ν*	*0.37*
Transverse shear modulus G_{23}, GPa	*10.7*		
In-plane Poisson's ratio ν_{12}	*0.26*		
Transverse Poisson's ratio ν_{23}	*0.39*		
Strength properties			
Tensile strength, MPa	*4210*	*Tensile strength, MPa*	*90*
Compressive strength, MPa	*2616*	*Compressive strength, MPa*	*148*
Shear strength, MPa	*-NA-*	*Shear strength, MPa*	*63*

Note: *T300 JB carbon material strength properties are taken from TORAYCA technical datasheet No: CFA-002.*
PPS material properties are taken from TECHTRON & RYTRON PPS data sheet.

Table 3. Homogenized elastic properties of the carbon-PPS impregnated yarn.

$\phi_f = 0.7$	E_{11}, [GPa]	E_{22}, [GPa]	G_{12}, [GPa]	G_{23}, [GPa]	ν_{12}	ν_{23}
Chamis micro mechanical homogenization	*162.60*	*13.70*	*6.50*	*5.07*	*0.29*	*0.35*
CCA[17] Concentric Cylindrical Assemblage	*162.20*	*15.0*	*6.20*	*-*	*0.28*	*0.40*

Table 4. Computed homogenized elastic constants of the carbon-PPS satin weave unit cell.

	PBC and Volume averaging	*Dirichlet BC's and Surface reactions*	*Method of Inclusions (Analytical)*	*Experiment*
E_{11}, *GPa*	*56.49*	*59.5*	*61.7*	57 ± 1
E_{22}, *GPa*	*56.41*	*59.5*	*61.7*	*-NA-*
E_{33}, *GPa*	*10.53*	*10.55*	*10.56*	*-NA-*
ν_{12}	*0.08*	*0.057*	*0.053*	0.05 ± 0.02
ν_{13}	*0.41*	*0.41*	*0.44*	*-NA-*
ν_{23}	*0.41*	*0.41*	*0.44*	*-NA-*
G_{12} *MPa*	*4280*	*4305*	*4297*	*4175[35]*
G_{13}, *MPa*	*3048*	*3286*	*3375*	*-NA-*
G_{23}, *MPa*	*3045*	*3286*	*3375*	*-NA-*

Table 5. Homogenized strength properties of the carbon-PPS impregnated yarn.

Mechanical property	*Carbon-PPS impregnated yarn* (ϕ_f *=0.7)*
Tensile strength, MPa	$F_L^t = 2947$ $F_T^t = 80$ $F_Z^t = 80$
Compressive strength, MPa	$F_L^c = 1832$ $F_T^c = 130$ $F_Z^c = 130$
Shear strength, MPa	$F_{TZ}^s = 56$ $F_{ZL}^s = 56$ $F_{LT}^s = 56$

Table 6. The characteristics of anisotropic damage model for fiber bundle and isotropic damage model for matrix[27].

	Anisotropic Damage Model for Fiber Bundle				
Damage Mode	*Mode L* 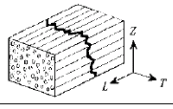	*Mode T & LT* 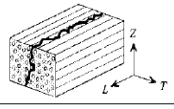	*Mode Z & ZL* 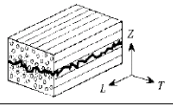	*Mode TZ* 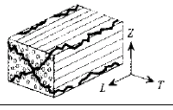	**Isotropic Damage Model for Matrix**
Maximum stress-to-strength ratio	$\frac{\sigma_L^2}{F_L^t F_L^c}$	$\frac{\sigma_T^2}{F_T^t F_T^c}$ or $\left(\frac{\tau_{LT}}{F_{LT}^s}\right)^2$	$\frac{\sigma_Z^2}{F_Z^t F_Z^c}$ or $\left(\frac{\tau_{ZL}}{F_{ZL}^s}\right)^2$	$\left(\frac{\tau_{TZ}}{F_{TZ}^s}\right)^2$	–
Damage tensor					
$\begin{bmatrix} D_L & 0 & 0 \\ 0 & D_T & 0 \\ 0 & 0 & D_Z \end{bmatrix}$	$\begin{bmatrix} 1 & 0 & 0 \\ 0 & 0 & 0 \\ 0 & 0 & 0 \end{bmatrix}$	$\begin{bmatrix} 0 & 0 & 0 \\ 0 & 1 & 0 \\ 0 & 0 & 0 \end{bmatrix}$	$\begin{bmatrix} 0 & 0 & 0 \\ 0 & 0 & 0 \\ 0 & 0 & 1 \end{bmatrix}$	$\begin{bmatrix} 0 & 0 & 0 \\ 0 & 1 & 0 \\ 0 & 0 & 1 \end{bmatrix}$	$\begin{bmatrix} 1 & 0 & 0 \\ 0 & 1 & 0 \\ 0 & 0 & 1 \end{bmatrix}$

Table 7. Local stress distribution on the weft yarn cross sections at the damage initiation strain.

	In-plane transverse stress, MPa (edge/ centre of the yarn)	*Normal out-of-plane stress, MPa (edge/ centre of the yarn)*	*Out-of-plane shear stress, MPa (edge/ centre of the yarn)*
CASE I (Inside the laminate)	*49/31*	*14/14*	*22/2*
CASE II-Single unit cell-2D pbc (on the surface)	*49/78*	*Negligible*	*16/7*
CASE II-8 unit cell stack (on the surface)	*62/75*	*Negligible*	*4/18*
CASE II-8 unit cell stack (inside the laminate)	*55/60*	*8/12*	*15/15*

a)

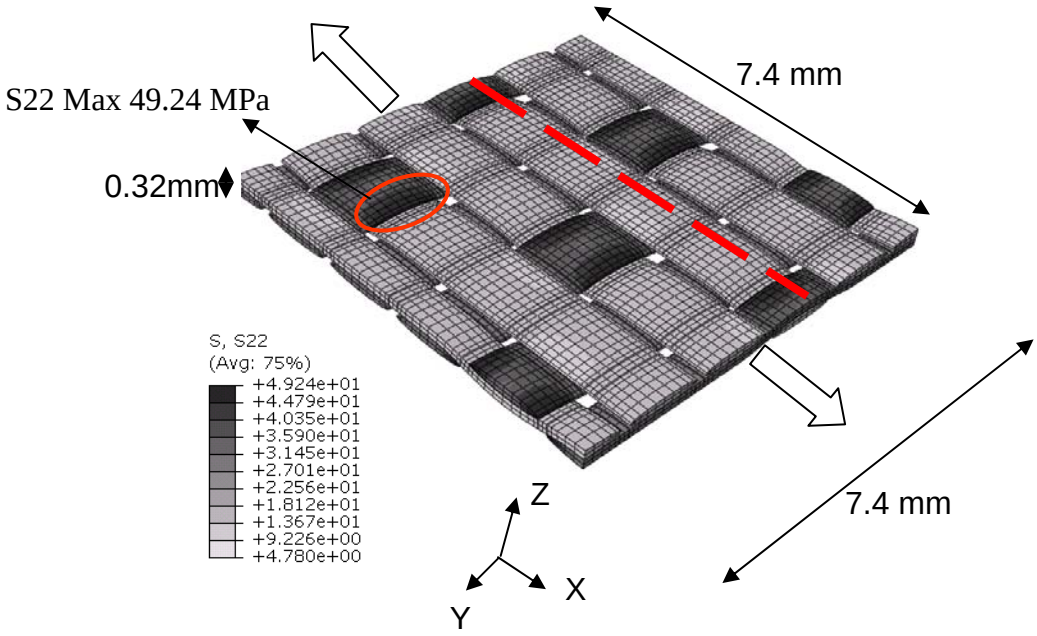
S22 Max 49.24 MPa
0.32mm
7.4 mm
7.4 mm
S, S22
(Avg: 75%)
+4.924e+01
+4.479e+01
+4.035e+01
+3.590e+01
+3.145e+01
+2.701e+01
+2.256e+01
+1.812e+01
+1.367e+01
+9.226e+00
+4.780e+00
Z
X
Y

b)

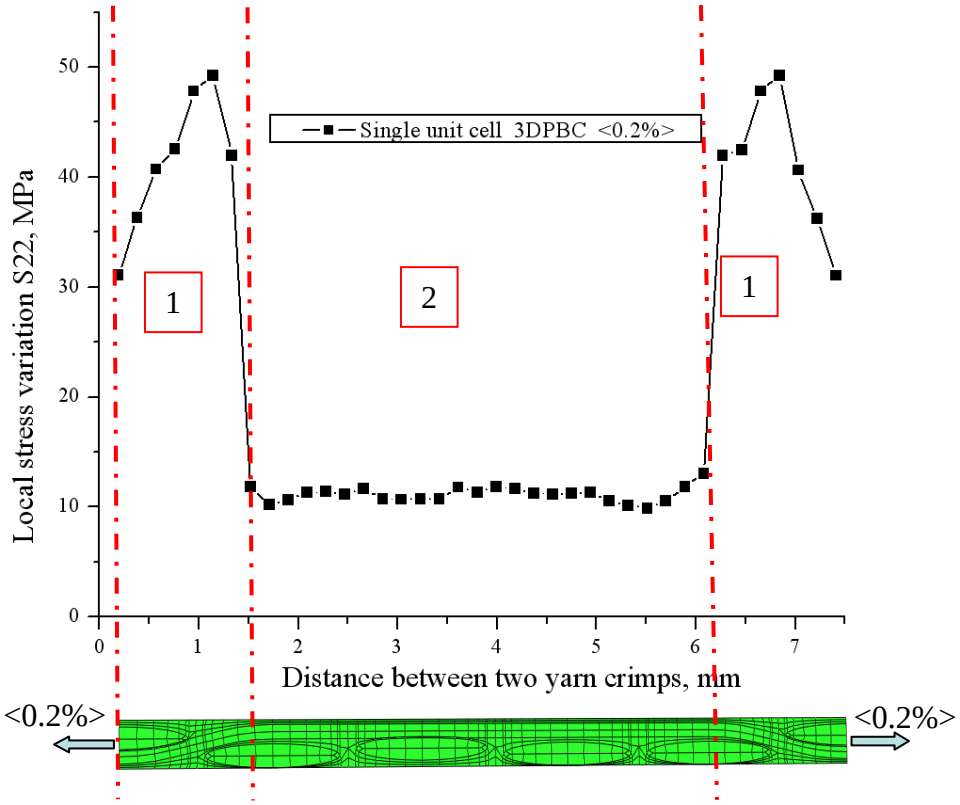
Single unit cell 3DPBC <0.2%>
Local stress variation S22, MPa
Distance between two yarn crimps, mm
1
2
1
<0.2%>
<0.2%>

c)

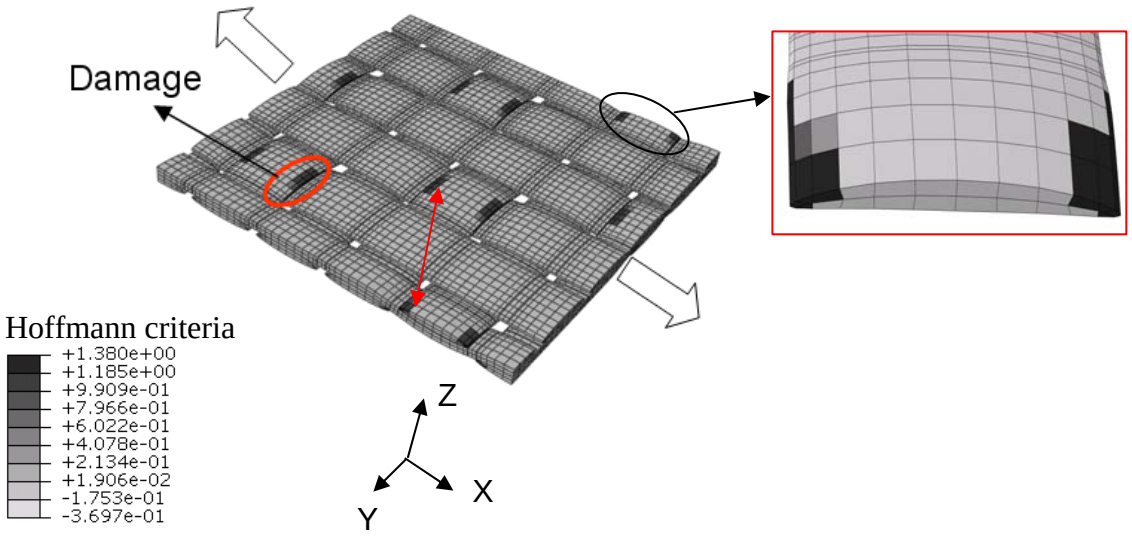

Figure 1. *Single unit cell with infinite laminate boundary conditions : a) transverse stress distribution on the weft yarn; b) transverse stress profile between two yarn crimp; c) transverse damage on the weft yarn at the yarn crimp location <0.2%>.*

a)

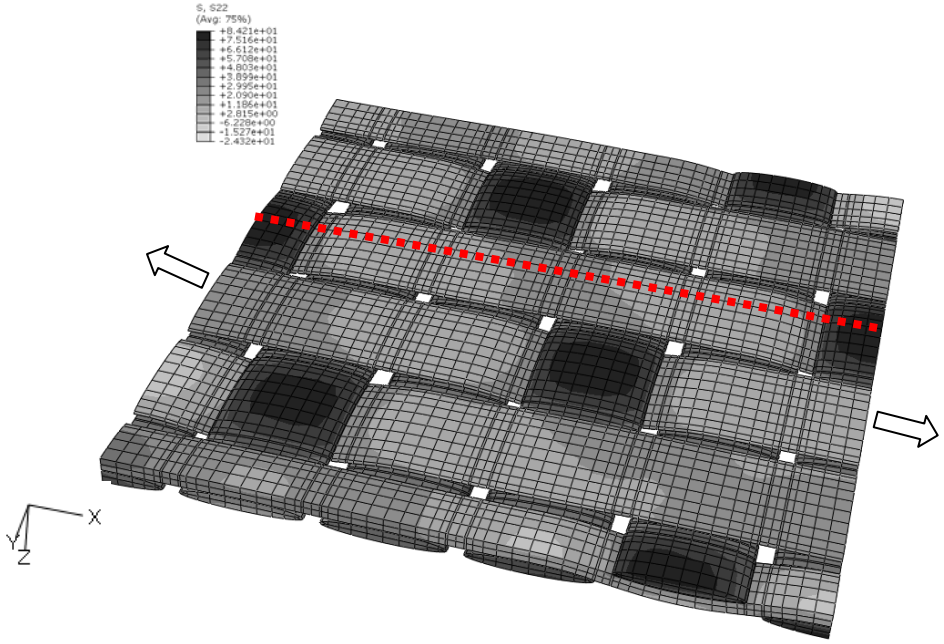
S, S22
(Avg: 75%)
+8.421e+01
+7.516e+01
+6.612e+01
+5.708e+01
+4.803e+01
+3.899e+01
+2.995e+01
+2.090e+01
+1.186e+01
+2.815e+00
-6.229e+00
-1.527e+01
-2.432e+01
X
Y
Z

b)

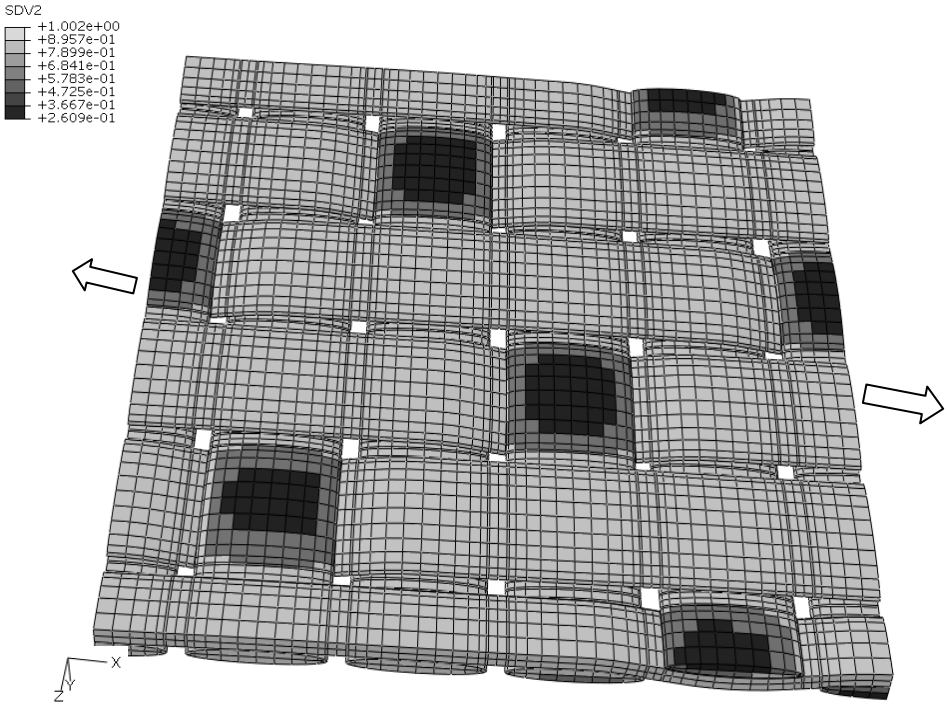
SDV2
+1.002e+00
+8.957e-01
+7.899e-01
+6.841e-01
+5.783e-01
+4.725e-01
+3.667e-01
+2.609e-01
X
Y
Z

c)

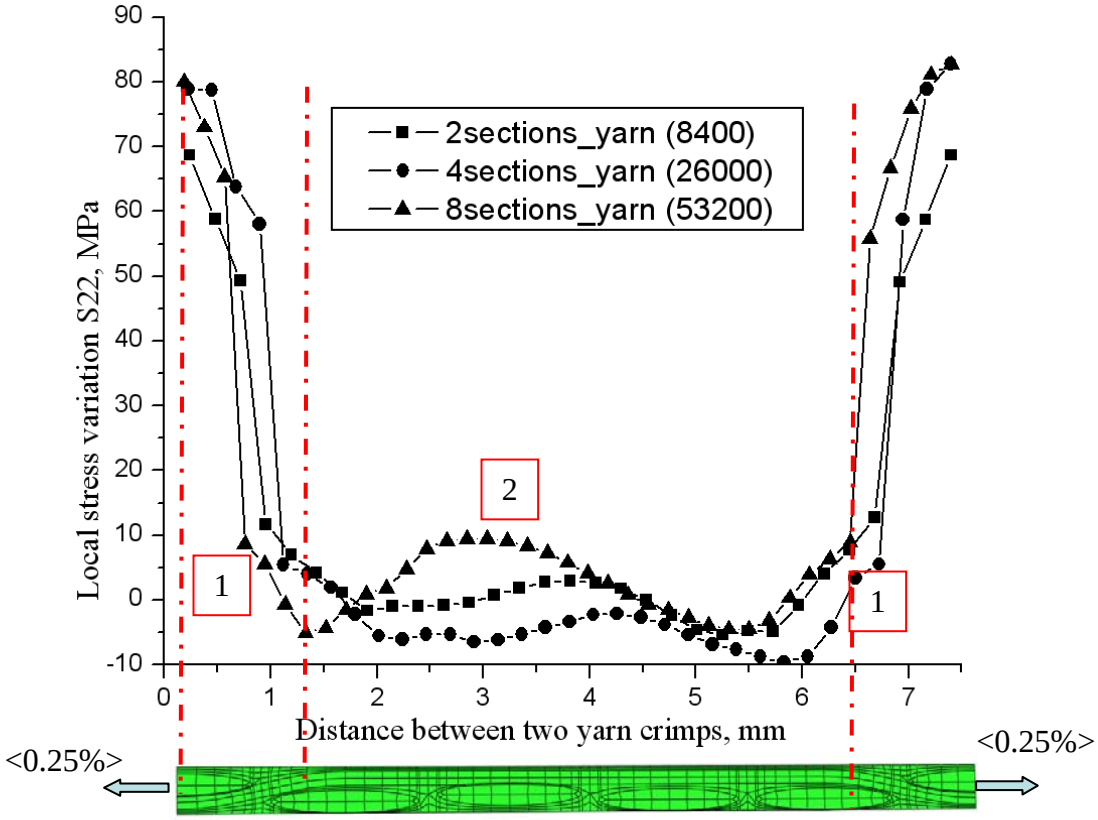

Figure 2. *Single unit cell stress and damage profiles with in-plane PBC: a) Transverse stress distribution on the weft yarn; b) Transverse damage on the weft yarn at the yarn crimp location c) Transverse stress profiles between two yarn crimps with different mesh size.*

a)

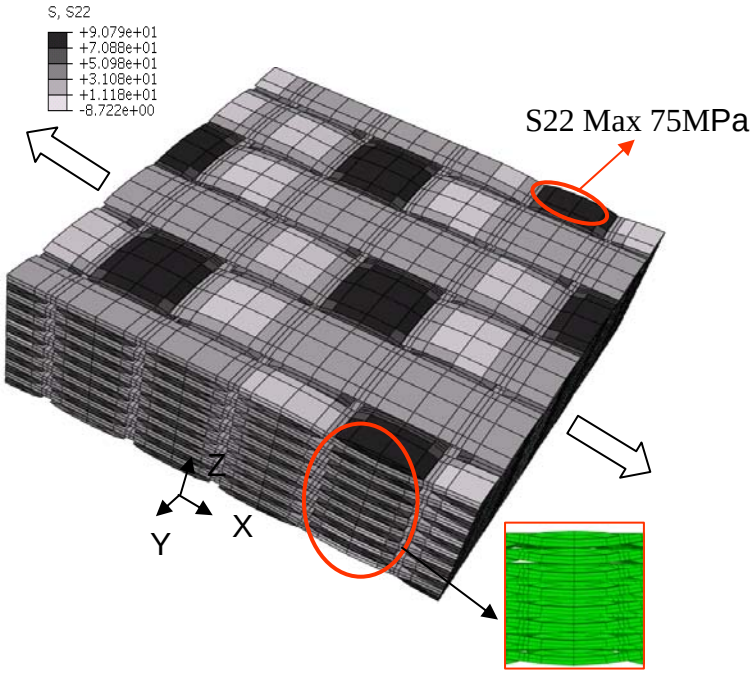

b)

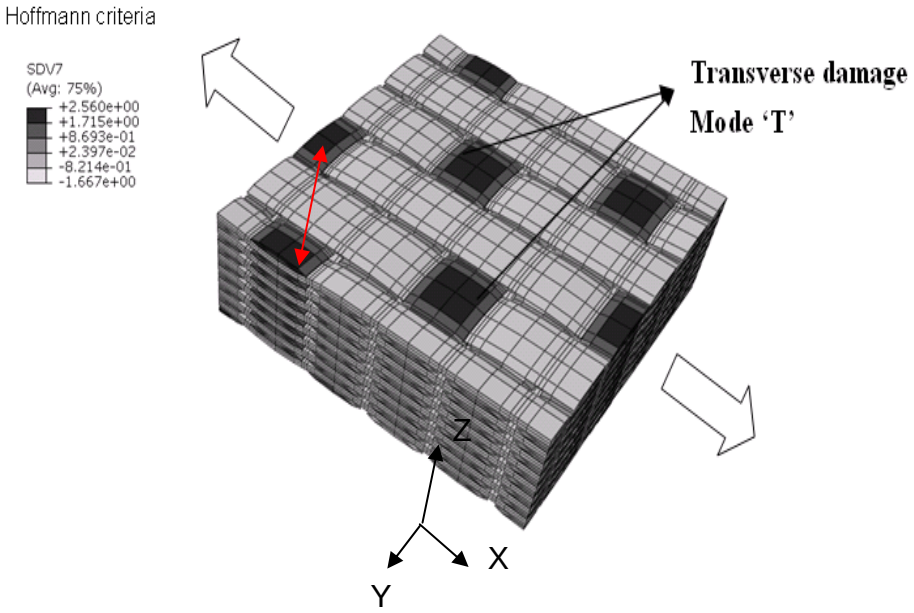

Figure 3. *8 unit cell stack FE analysis : a) Transverse stress distribution on the weft yarn; b) Transverse damage locations on the weft yarn at the yarn crimp location <0.44%> with the 8 unit cell in-phase stack, in-plane PBC.*

a)

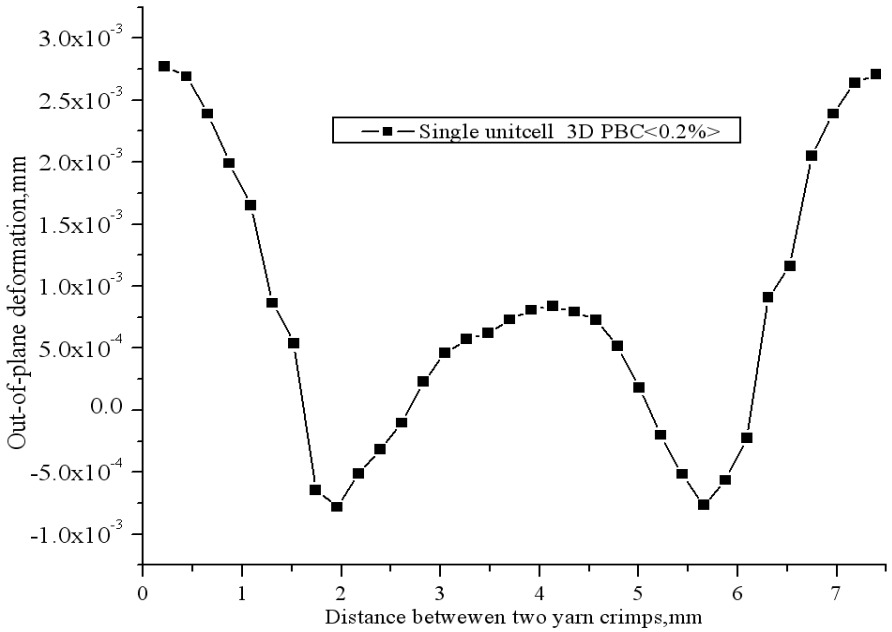
Single unitcell 3D PBC<0.2%>
Out-of-plane deformation,mm
Distance betwewen two yarn crimps,mm
3.0x10-3
2.5x10-3
2.0x10-3
1.5x10-3
1.0x10-3
5.0x10-4
0.0
-5.0x10-4
-1.0x10-3
0
1
2
3
4
5
6
7

b)

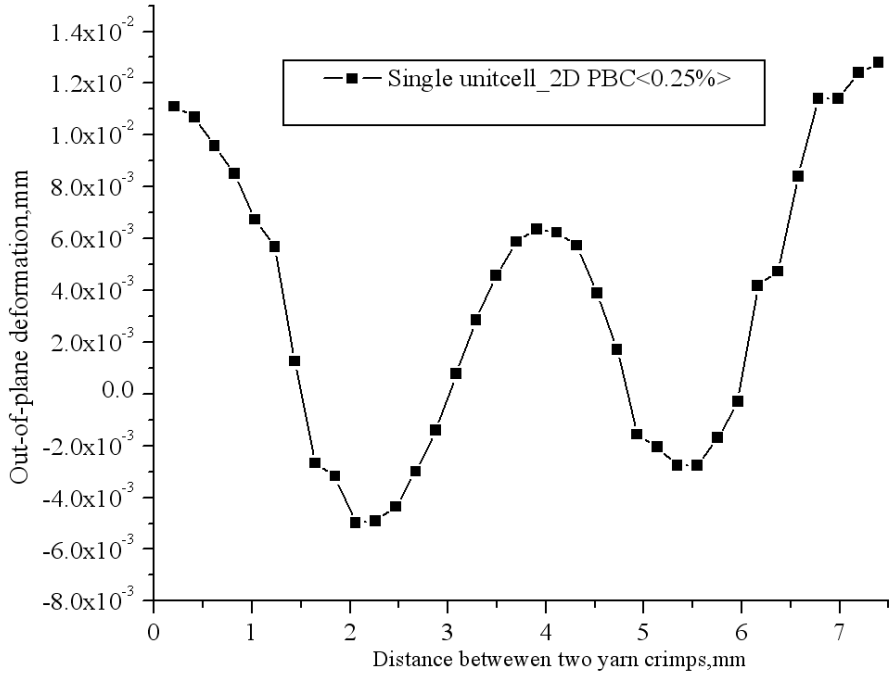
Single unitcell_2D PBC<0.25%>
Out-of-plane deformation,mm
Distance betwewen two yarn crimps,mm
1.4x10-2
1.2x10-2
1.0x10-2
8.0x10-3
6.0x10-3
4.0x10-3
2.0x10-3
0.0
-2.0x10-3
-4.0x10-3
-6.0x10-3
-8.0x10-3
0
1
2
3
4
5
6
7

c)

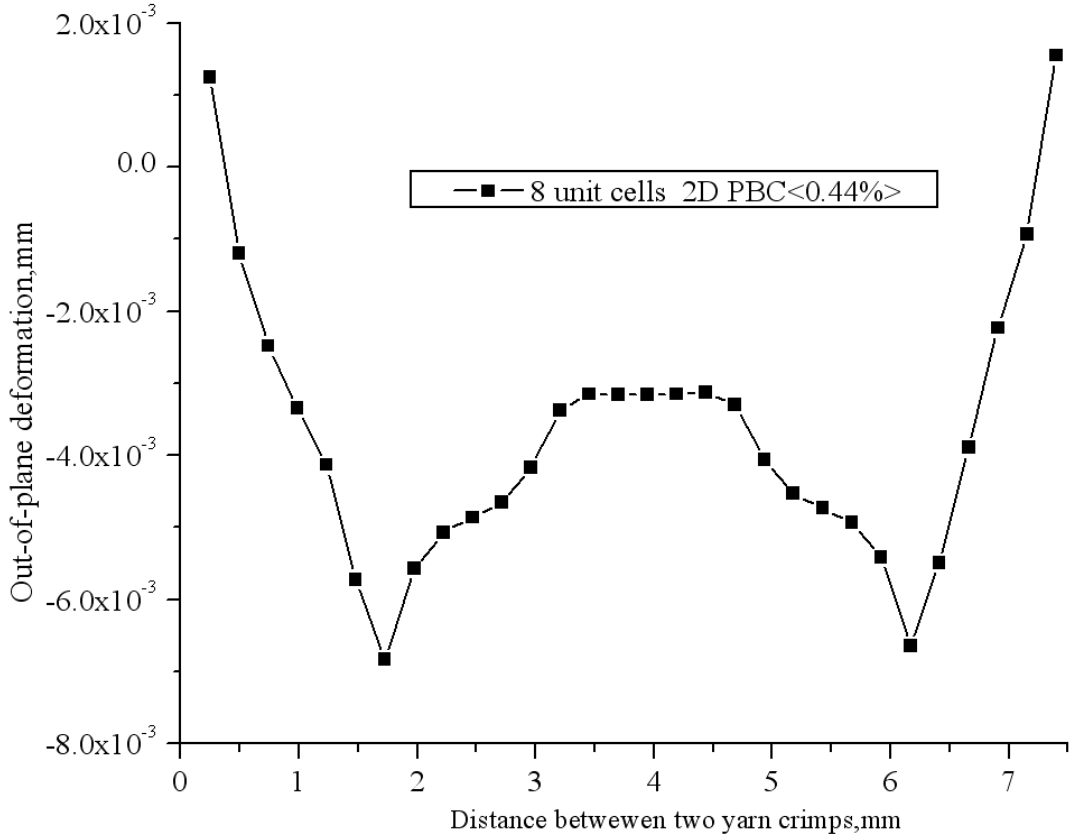

Figure 4. *Out-of-plane deformation of the unit cells: a) single unit cell with 3D PBC (<0.2%>); b) single unit cell with 2D PBC (<0.25%>); c) 8 unit cell stack with 2D PBC (<0.44%>).*